Electronic Supplementary Material (ESI) for Soft Matter.

Supporting Information for

Structure, Viscoelasticity, and Interfacial Dynamics of a Model Polymeric Bicontinuous Microemulsion

Robert J. Hickey,[1] Timothy M. Gillard,[2] Matthew T. Irwin,[2] Timothy P. Lodge,[1,2] and Frank S. Bates[2]

[1]Department of Chemistry and [2]Department of Chemical Engineering and Materials Science, University of Minnesota, Minneapolis, MN 55455

SAXS Heating and Cooling Ramps for the BμE

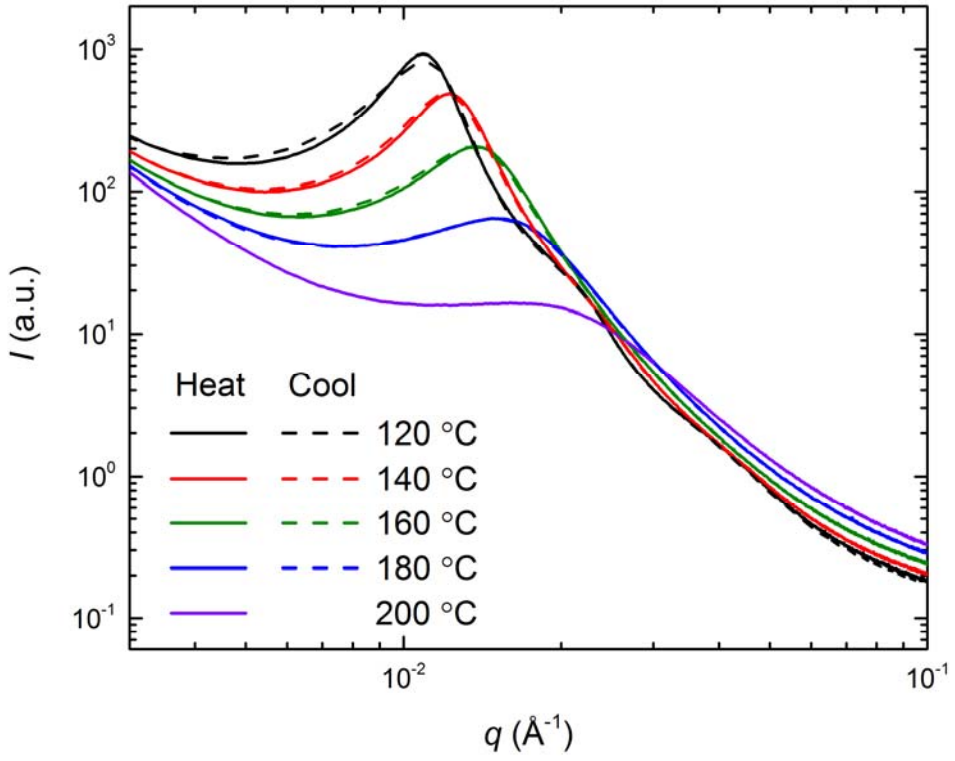

Figure S1. SAXS heating and cooling temperature ramps for the BμE. The sample was initially annealed at 120 °C for 16 h. On cooling, there is hysteresis at lower temperatures, which is attributed to the temperature dependent structural relaxation mechanism as explained in the main text.

BμE Rheology Data

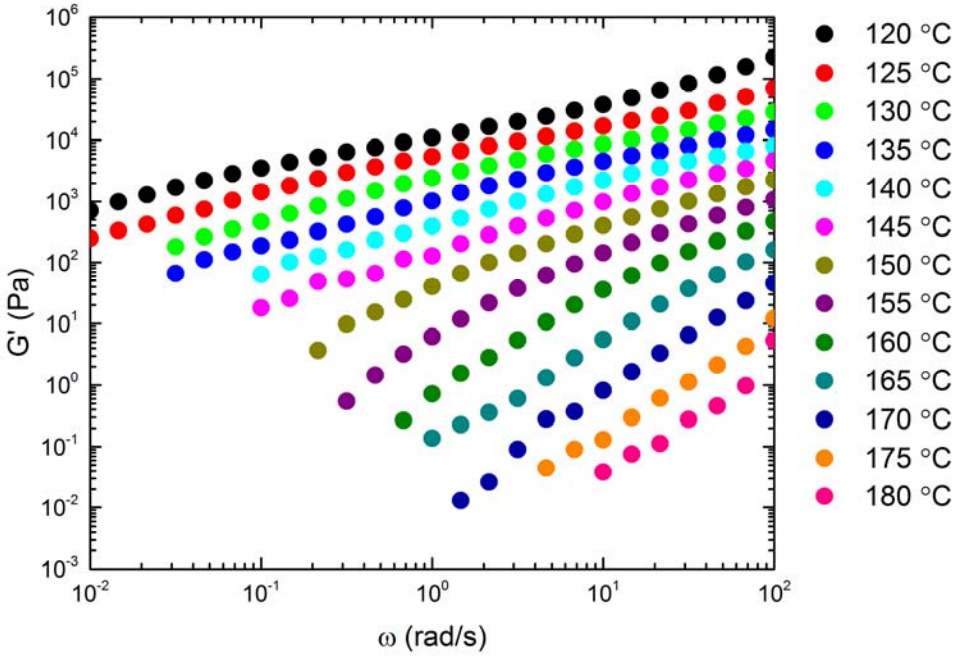

Figure S2. Plot of the storage (*G*') modulus for the BμE as a function of frequency. Data were obtained from frequency sweeps at various temperatures and strain % values listed in Table S1.

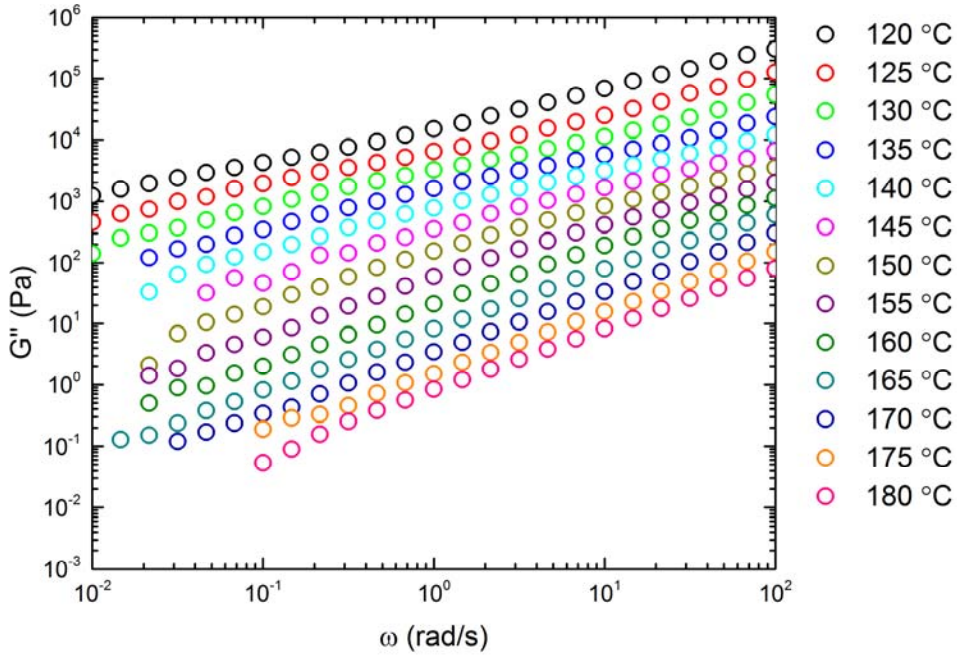

Figure S3. Plot of the loss (*G*") modulus for the BμE as a function of frequency. Data were obtained from frequency sweeps at various temperatures and strain % values listed in Table S1.

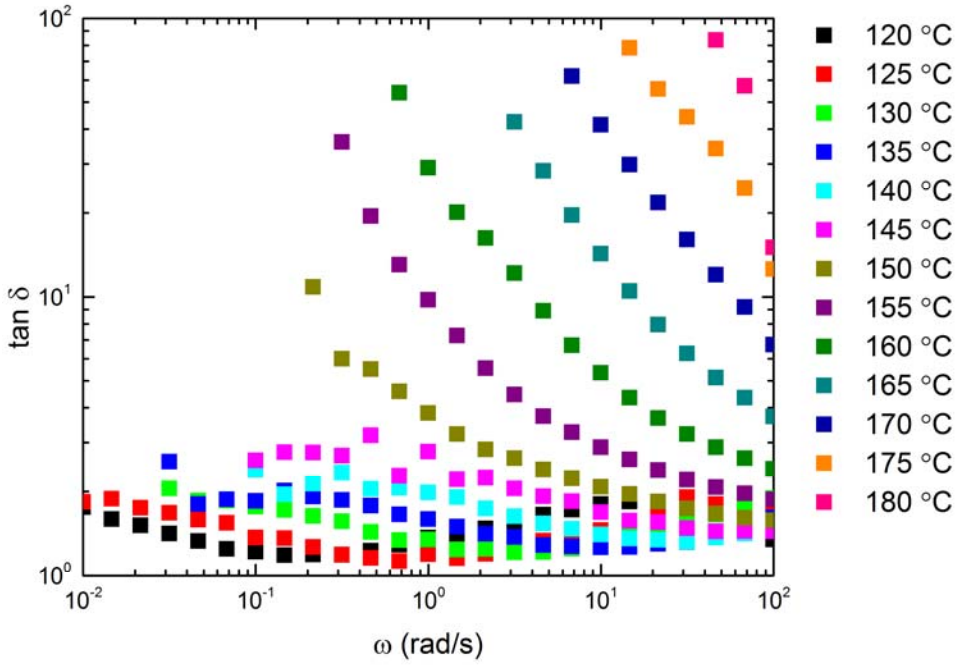

Figure S4. Plot of tan δ for the BμE as a function of frequency. Data were obtained from dynamic frequency sweeps at various temperatures and strain % values listed in Table S1.

Table S1. The strain (%) and shift factors (a_T) used for the time-temperature superposition for the BμE.

Temperature (°C)	Strain (%)	a_T
120	0.04	150
125	0.04	40
130	0.06	12
135	0.08	3.3
140	0.1	1
145	0.5	0.35
150	1.0	0.12
155	5.0	0.04
160	10.0	0.015
165	30.0	0.005
170	40.0	0.002
175	45.0	0.0009
180	50.0	0.0005

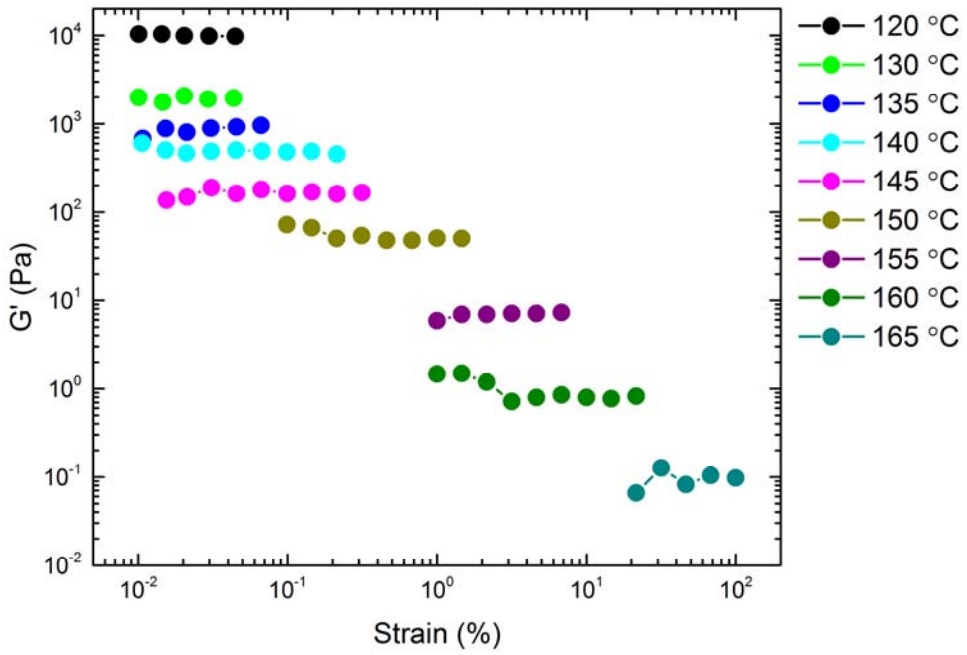

Figure S5. Plot of the storage (*G*') modulus for the BμE as a function of strain amplitude. Data were obtained from strain sweeps at the indicated temperatures.

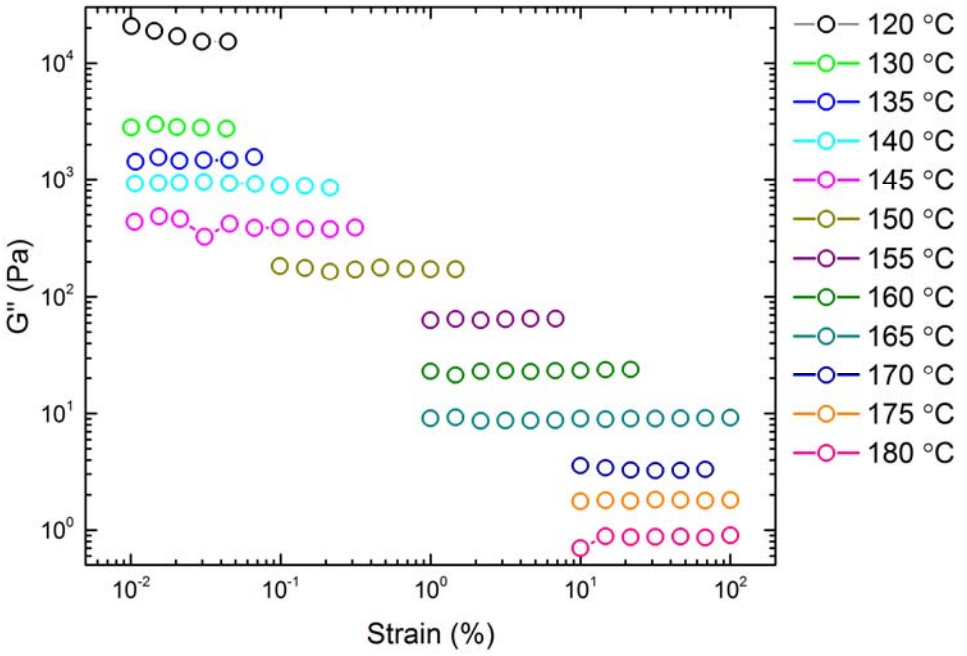

Figure S6. Plot of the loss (*G*") modulus for the BμE as a function of strain amplitude. Data were obtained from strain sweeps at the indicated temperatures.

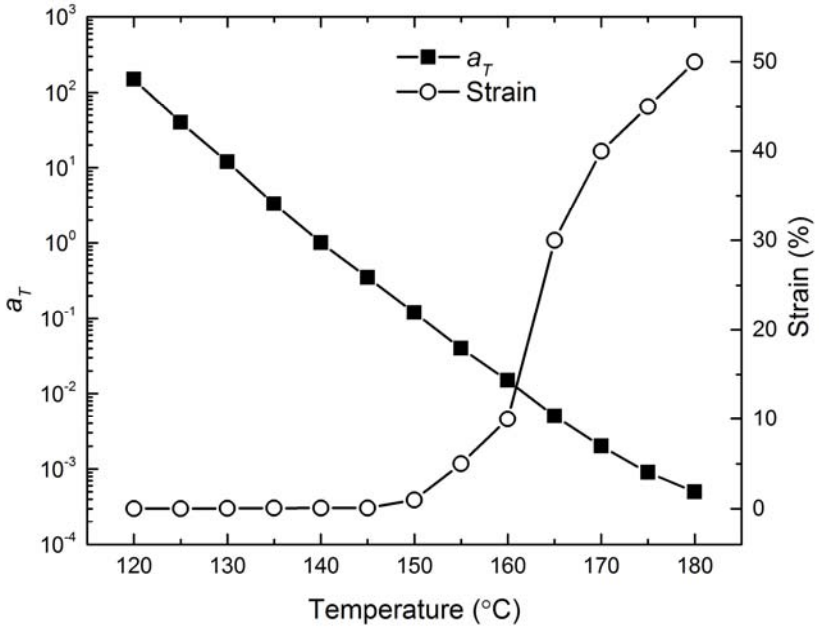

Figure S7. Shift factors (a_T) and applied strain for the BμE as a function of temperature. The increase in strain at elevated temperatures is due to a decrease in the modulus (Figures S5 and S6 demonstrate we are still in the linear regime).

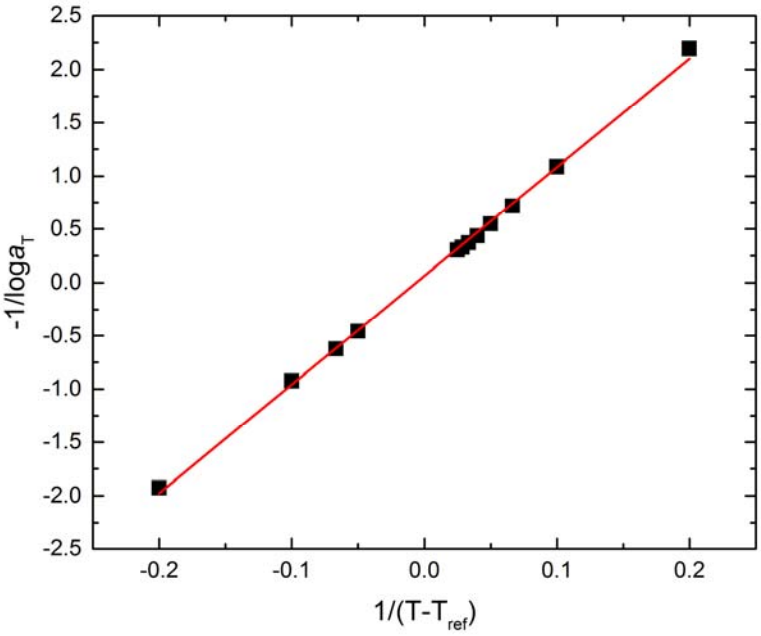

Figure S8. Linear WLF fit for the BμE. The reference temperature is 140 °C. The WLF parameters were calculated to be C_1 = 16.09 and C_2 = 164.13 ºC.

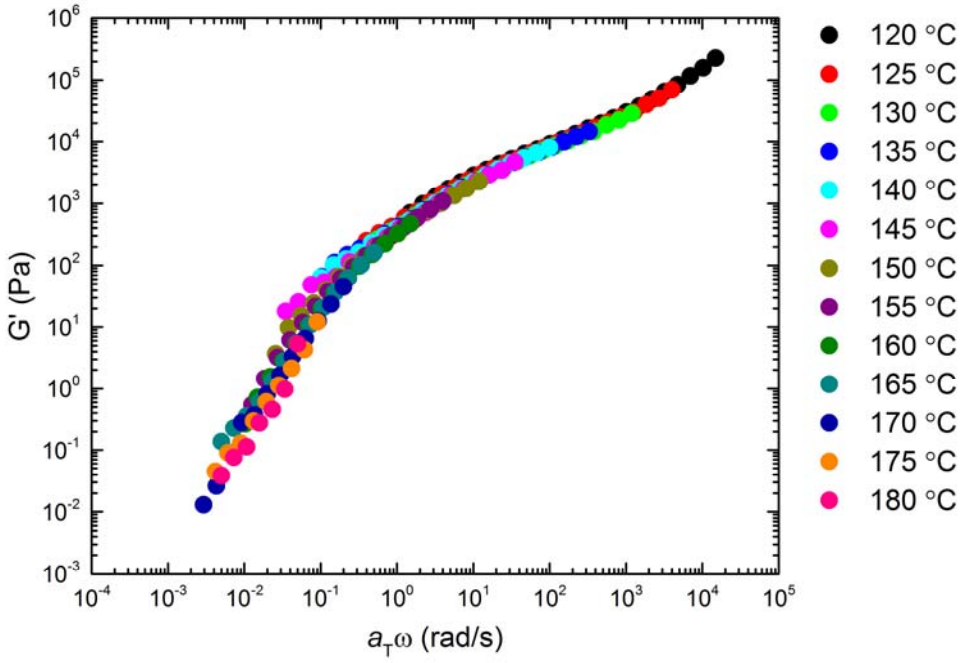

Figure S9. The tTS master curve for the storage (G') modulus for the BμE. Shift factors (a_T) were applied with a reference temperature of 140 °C and C_1 = 16.09 and C_2 = 164.13 ºC.

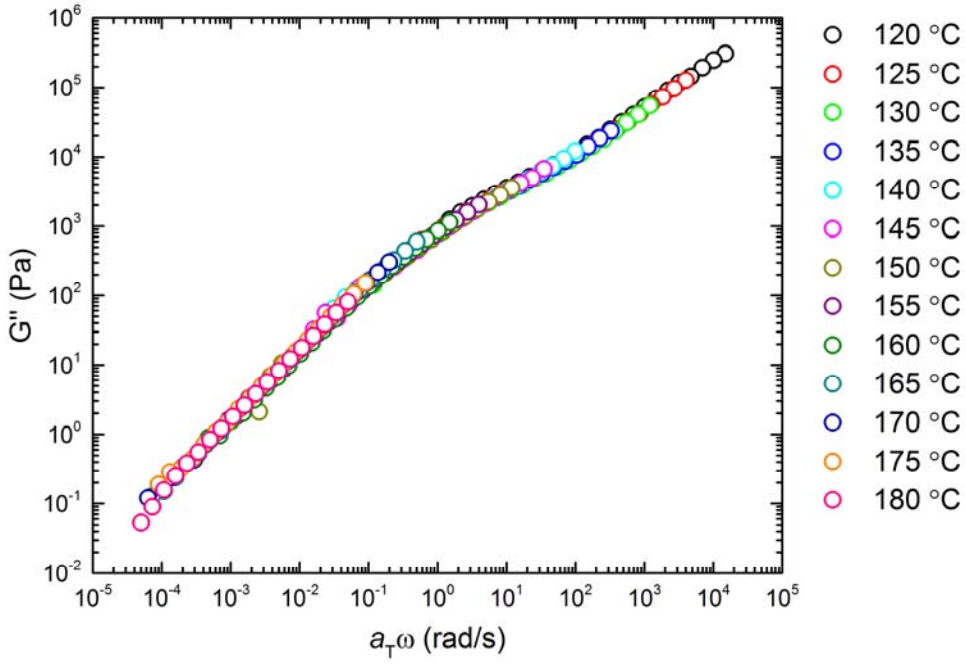

Figure S10. The tTS master curve for the loss (G'') modulus for the BμE. Shift factors (a_T) were applied with a reference temperature of 140 °C and C_1 = 16.09 and C_2 = 164.13 ºC.

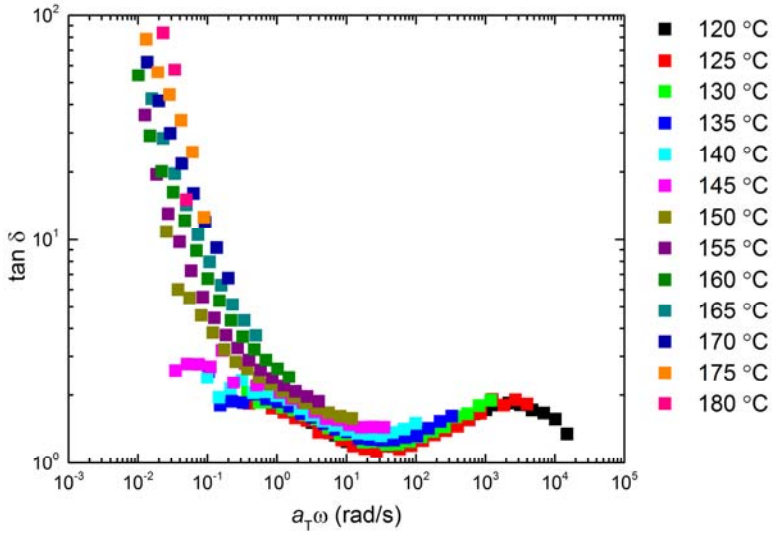

Figure S11. The tTS master curve of tan δ for the BμE. Shift factors (a_T) were applied with a reference temperature of 140 °C and C_1 = 16.09 and C_2 = 164.13 ºC.

PCHE Homopolymer Rheology Data

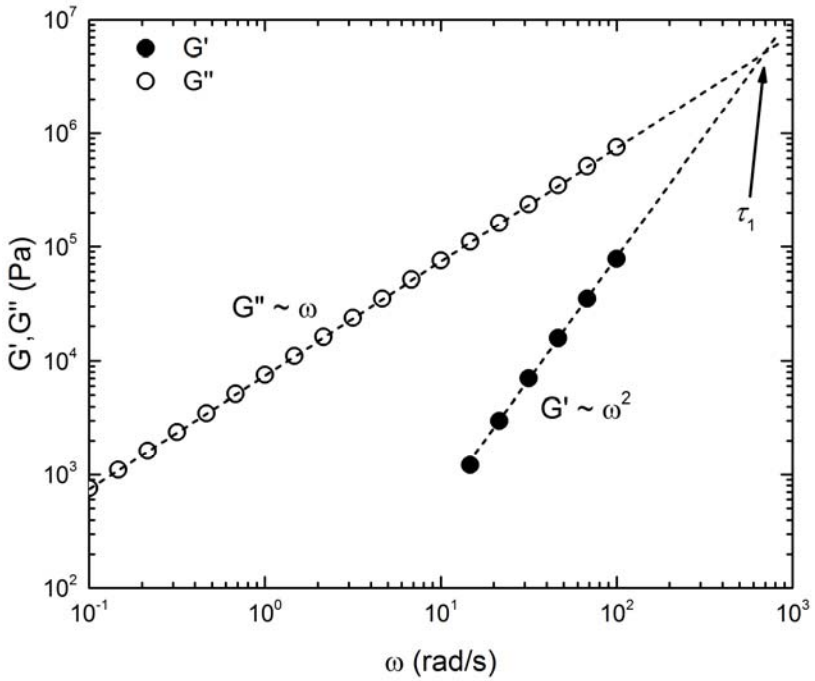

Figure S12. Plot of the storage (G') and loss (G'') moduli for PCHE as a function of frequency at 145 °C. The longest relaxation time (τ_1) for PCHE (2.6 kg/mol) was calculated to be 0.001 s using the relationship where $\tau_1 = G'/(G''\omega)$ in the terminal regime ($\omega \rightarrow 0$).

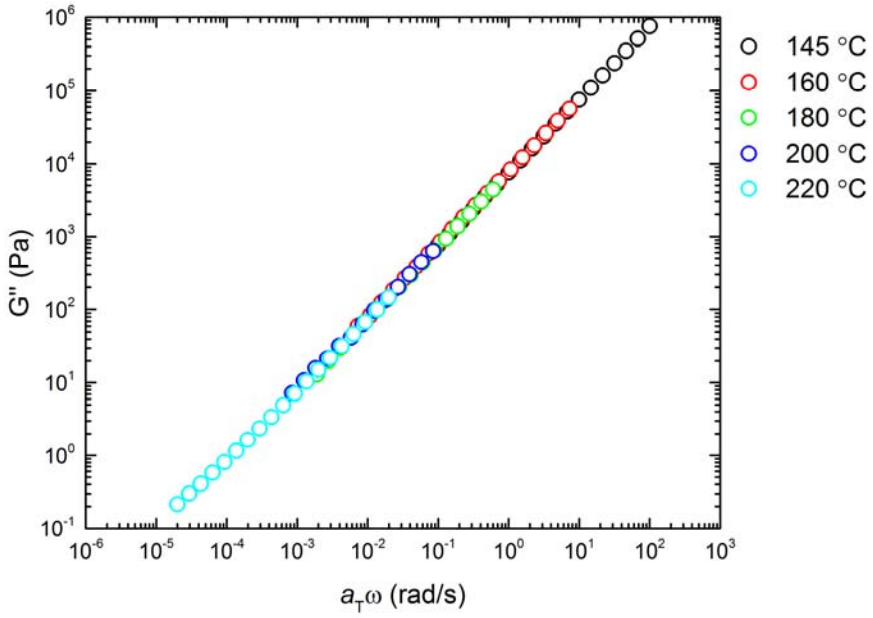

Figure S13. The tTS master curve for the loss (G'') modulus for PCHE. Shift factors (a_T) were applied to the frequency with a reference temperature of 145 °C and C_1 = 8.36 and C_2 = 95.40 ºC.

PE Homopolymer Rheology Data

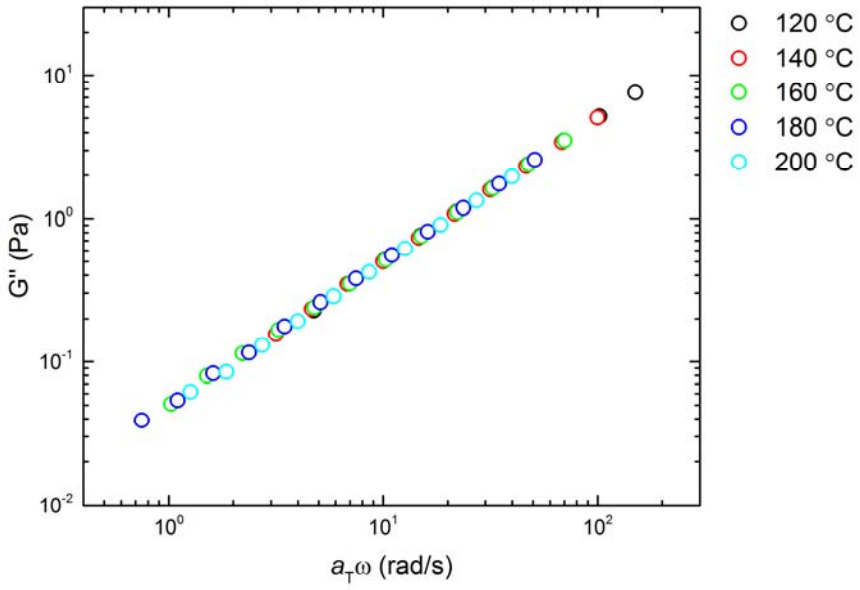

Figure S14. The tTS master curve for the loss (G'') modulus for PE. Shift factors (a_T) were applied with a reference temperature of 140 °C and C_1 = 2.43 and C_2 = 294.67 ºC.

Shifting BμE Rheology Data using WLF Parameters from PCHE and PCHE-PE-14

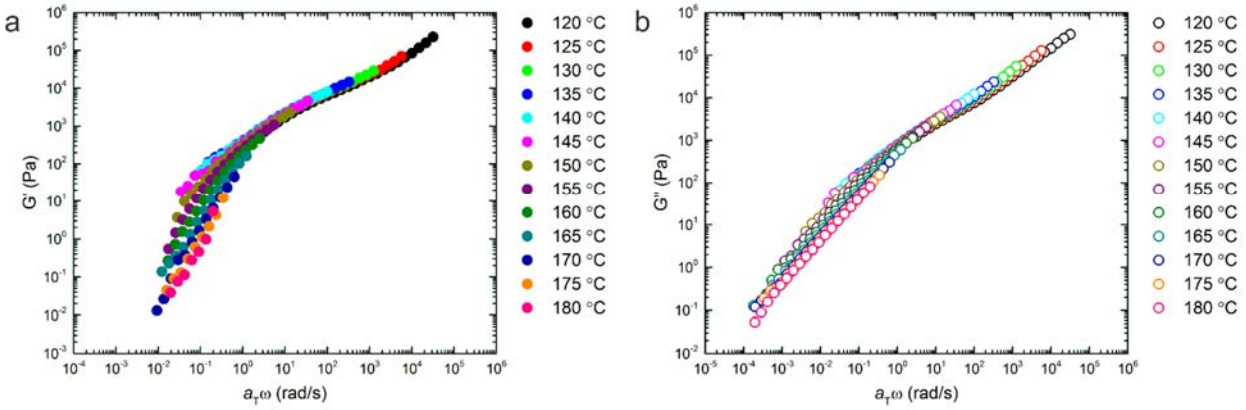

Figure S15. Master plots of the (a) storage (*G*') and (b) loss (*G*") moduli for the BμE using WLF parameters calculated from the PCHE homopolymer. The values used were C_1 = 8.82 and C_2 = 90.40 ºC, with a reference temperature of 140 °C.

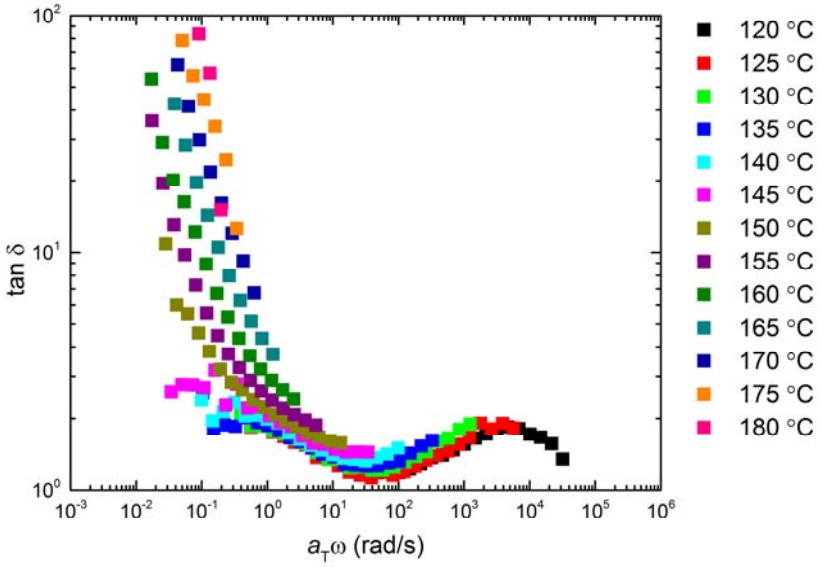

Figure S16. The tTS master curve of tan δ for the BμE using WLF parameters calculated from the PCHE homopolymer. The values used were C_1 = 8.82 and C_2 = 90.40 ºC, with a reference temperature of 140 °C.

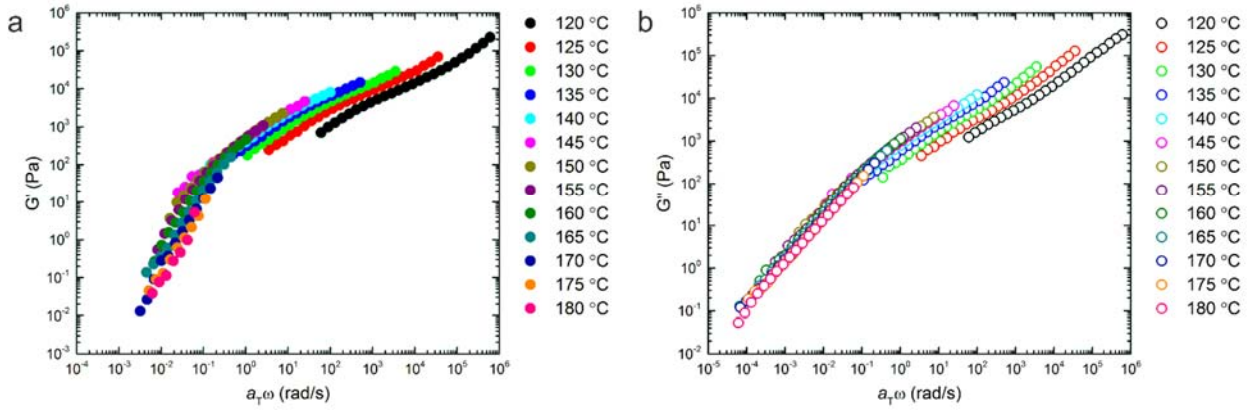

Figure S17. Master plots of the (a) storage (G') and (b) loss (G'') moduli for the BμE using WLF parameters calculated from PCHE-PE-14. The values used were C_1 = 8.37 and C_2 = 64.25 ºC, with a reference temperature of 140 °C.

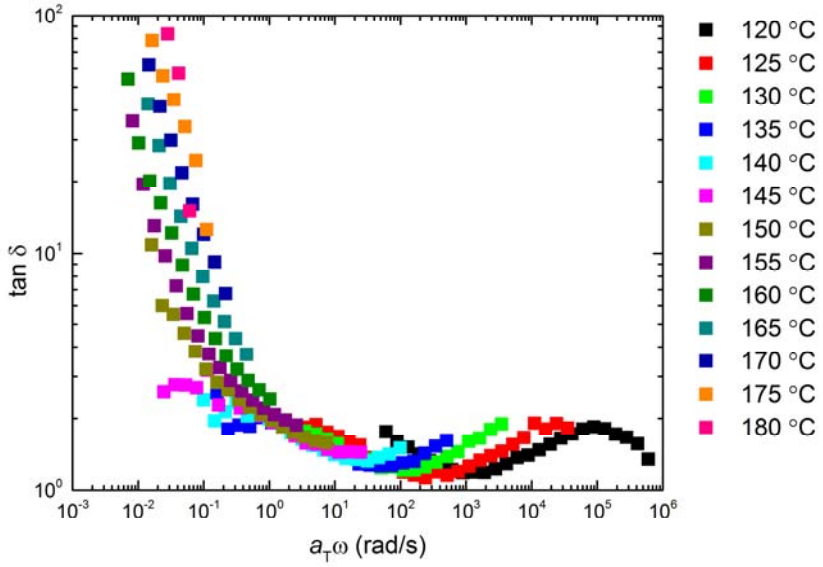

Figure S18. The tTS master curve of tan δ for the BμE using WLF parameters calculated from PCHE-PE-14. The values used were C_1 = 8.37 and C_2 = 64.25 ºC, with a reference temperature of 140 °C

Comparing 90 – δ of the BμE and PCHE-PE-14

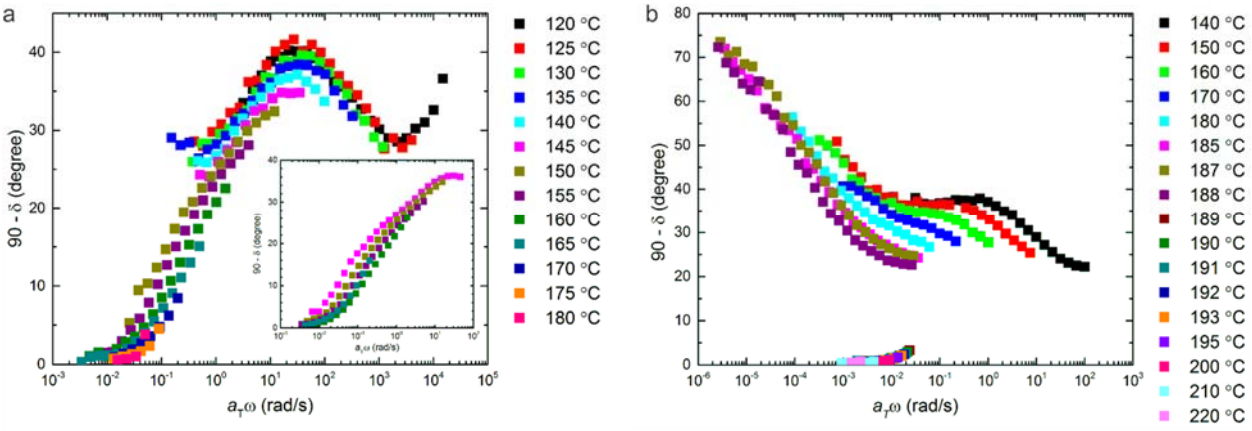

Figure S19. tTS master curves of phase angle (90 – δ) for the (a) BμE and (b) PCHE-PE-14. Shift factors (a_T) were applied with a reference temperature of 140 °C. (a) Inset highlights interfacial fluctuations in the terminal regime that were measured by extending the frequency region using a stress controlled TA Instruments Discovery Hybrid Rheometer.

van Gurp-Palmen Plot of the BμE

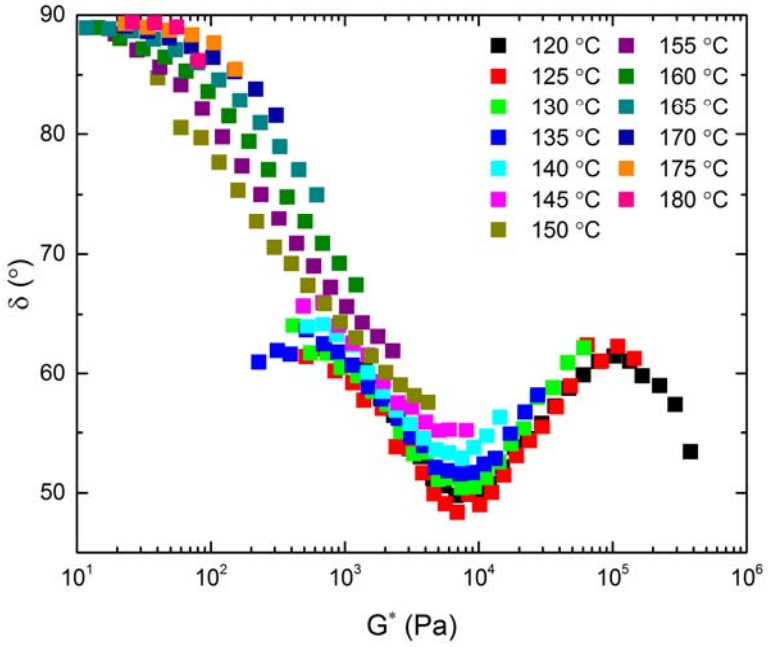

Figure S20. van Gurp-Palmen plot (phase angle (δ) *vs.* complex modulus(G^*)) of the BμE.

Steady Shear Data for PCHE, PE, and BμE Samples

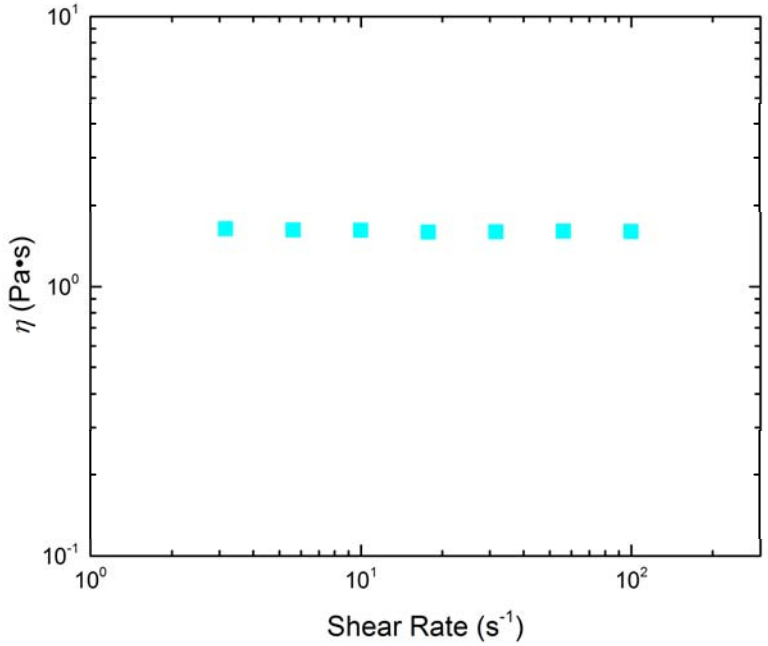

Figure S21. Steady shear data for PCHE at 220 °C. The viscosity (η) is the same as calculated from the in-phase complex viscosity ($\eta' = G''/\omega$) at 220 °C. The measurement time per rate was 3.5 min.

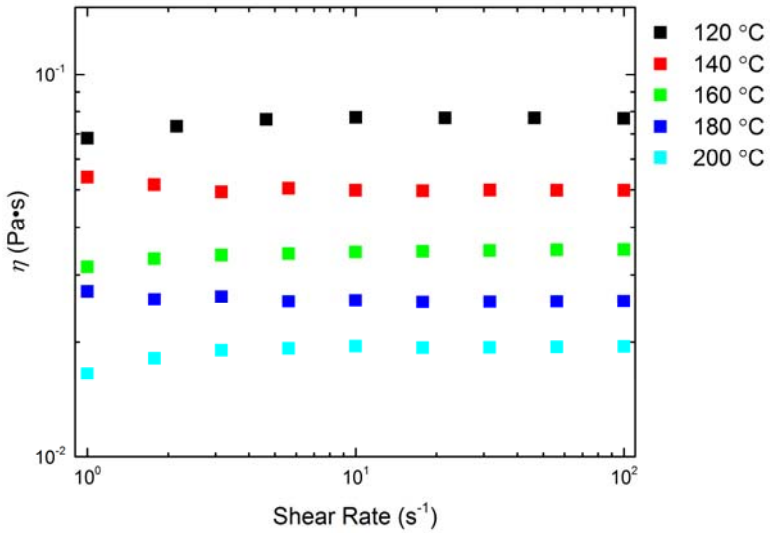

Figure S22. Steady shear data for PE at various temperatures. The viscosity (η) is the same as calculated from the in-phase dynamic viscosity ($\eta' = G''/\omega$) for temperatures in the range 120-200 °C. The measurement time per rate was 3.5 min.

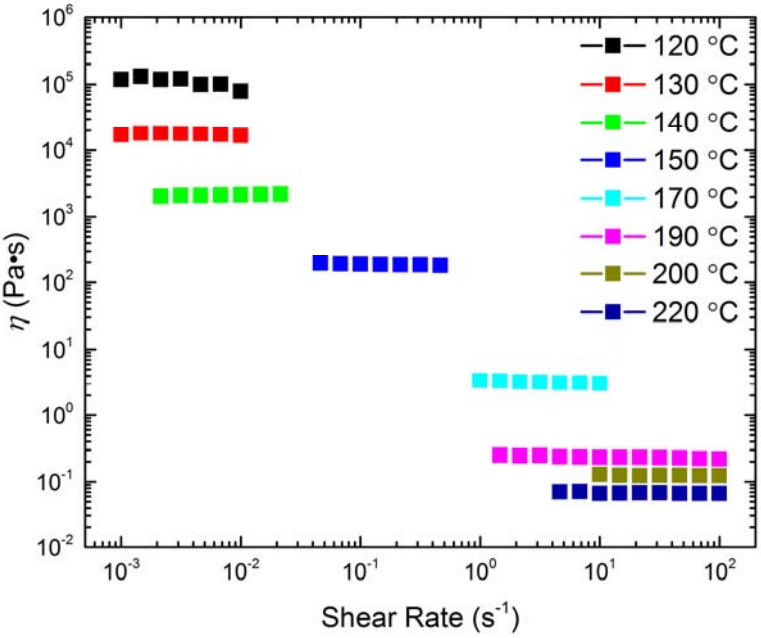

Figure S23. Steady shear experiments for the BμE in the temperature range 120 – 220 °C. The measurement time per rate was 3.5 min.

Analysis of the Extracted Fitting and Calculated Structural Parameters from the T-S Model

Table S2. Extracted fitting parameters from the T-S model for the BμE.

Temperature (°C)	a_2	c_1	c_2
125	0.0037 ± 0.0001	-48.5 ± 1.2	$1.81 \times 10^5 \pm 4.0 \times 10^3$
130	0.0042 ± 0.0001	-51.0 ± 1.4	$1.80 \times 10^5 \pm 5.0 \times 10^3$
140	0.0053 ± 0.0001	-56.7 ± 0.7	$1.79 \times 10^5 \pm 2.0 \times 10^3$
150	0.0070 ± 0.0001	-64.4 ± 1.0	$1.79 \times 10^5 \pm 3.0 \times 10^3$
160	0.0090 ± 0.0001	-69.0 ± 1.1	$1.71 \times 10^5 \pm 3.0 \times 10^3$
170	0.0110 ± 0.0001	-66.2 ± 1.3	$1.50 \times 10^5 \pm 3.0 \times 10^3$
180	0.0149 ± 0.0002	-63.6 ± 1.2	$1.35 \times 10^5 \pm 2.0 \times 10^3$
190	0.0262 ± 0.0006	-69.6 ± 4.4	$1.28 \times 10^5 \pm 8.0 \times 10^3$
200	0.0500 ± 0.0011	-75.7 ± 6.4	$1.19 \times 10^5 \pm 8.0 \times 10^3$

Table S3. Calculated structural parameters from the T-S model for the BμE.

Temperature (°C)	d (nm)	ξ (nm)	f_a
125	53.3 ± 0.4	45.6 ± 13.5	-0.93 ± 0.02
130	51.8 ± 0.5	43.5 ± 13.0	-0.93 ± 0.03
140	48.9 ± 0.2	38.7 ± 4.7	-0.92 ± 0.01
150	45.7 ± 0.3	33.1 ± 3.9	-0.91 ± 0.02
160	42.8 ± 0.3	27.2 ± 2.6	-0.88 ± 0.02
170	40.1 ± 0.3	20.1 ± 1.5	-0.82 ± 0.02
180	37.3 ± 0.2	14.4 ± 0.4	-0.71 ± 0.02
190	33.0 ± 0.6	10.5 ± 0.9	-0.60 ± 0.04
200	28.6 ± 0.7	7.8 ± 0.5	-0.49 ± 0.05

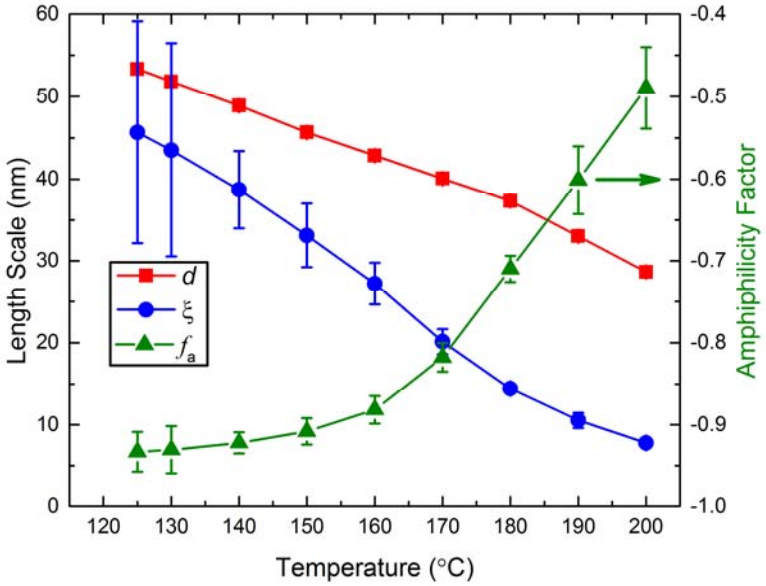

Figure S24. Plotted domain spacing (d), correlation length (ξ), and amphiphilicity factor (f_a) as a function of temperature with uncertainty values.

In general, the calculated structural parameters, domain spacing (d), correlation length (ξ), and amphiphilicity factor (f_a), are determined from the location (q (Å^{-1})), the width, and the intensity of the primary scattering peak, respectively. We determined the uncertainty in the values of the extracted fitting parameters from the least-squares method of the T-S fit. The error in the calculated structural parameters was then determined by propagating the error of the extracted fitting parameters. From the uncertainty analysis presented in Figure S24 and Tables S2 and S3 we find that the trends presented in this work are within the uncertainty of the calculated structural parameter values. In addition, the trends presented in Figure 5 of the main text are supported

independently with the calculated structural parameters from SAXS (Figure S25). Therefore, our conclusions are supported by our experimental data.

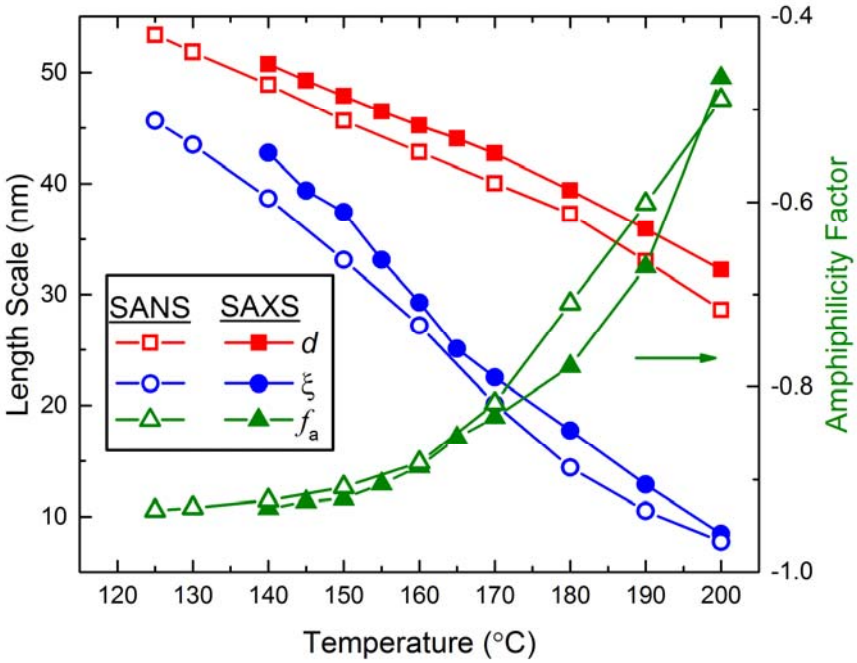

Figure S25. Comparison of calculated structural parameters, domain spacing (d), correlation length (ξ), and amphiphilicity factor (f_a), from SANS and SAXS as a function of temperature.